ISBN: 978-3-95450-211-0 doi:10.18429/JACoW-SRF2019-THP078

CERN'S SRF TEST STAND FOR CAVITY PERFORMANCE MEASUREMENTS

N. Stapley*, J. Bastard, M. Coly, A.E. Ivanov, A. Macpherson, N. Shipman, K. Turaj, CERN, Geneva, Switzerland
I. Ben-Zvi, Brookhaven National Laboratory BNL, New York, USA
A.Castilla, Lancaster University, Lancaster, United Kingdom
K. Hernandez-Chahin, Universidad de Guanajuato, Leon, Mexico
M. Wartak, A. Zwozniak, Institute of Nuclear Physics Polish Academy of Sciences, IFJ PAN, Krakow, Poland

Abstract

Recent deployment of a digital low-level RF (LLRF) system within the cavity-testing framework of CERN's vertical test cryostats has permitted a full revamp of cavity performance validation. With both full continuous and pulse mode operation, steady state and transient RF behavior can be effectively probed. Due to direct and integrated control and monitoring of environmental test conditions, standard and novel RF measurement procedures have been developed and integrated into the testing infrastructure, along with a coherent flow of high granularity measurement data. We present an overview of this cavity measurement system and address the underlying architectural structure, data handling and integration of user interfaces. In addition, we highlight the benefits of the variety of RF cavity measurements that can now be accommodated in our large 2 K cryostats.

INTRODUCTION

The CERN infrastructure for testing and validating superconducting RF cavities has recently undergone a full upgrade in order to allow for state-of-the-art RF measurements on both prototype and production SRF cavities. As part of this upgrade, both the electromechanical structure of the cryostat and the low-level RF operation has been addressed, with the resulting system now fully functional.

MECHANICAL SETUP

CERN's vertical test cryostats provide for operation down to 1.8K with forward RF power up to 250W. Design of the cryostat is such that cool down and filling with liquid helium is done from below the cavity, and distributed heater units allow for control of the vertical temperature gradient during initial cool down and through thermal cycling around the niobium superconducting transition.

In addition, the cryostats are fitted with active magnetic shielding and a full set of diagnostics systems to control the RF measurement environment. The ambient 3-vector magnetic field is typically supressed to below 50 nT and can be maintained with an active feedback loop during cool down if required.

Cavity installation on the cryostat insert is done such that the cavity is held with only one fixed point so to minimise insert related constraints on the Lorentz force detuning. Further, isolation washers and ceramic inserts on the cavity pumping line ensure the cavity is electrically isolated from the cryostat structure (Fig. 1), which allows for direct control and measurement of thermo-electric current during cool down. As an example, Fig. 2 shows first measurements of the thermo-electric current measured during the cool down of a 5-cell 704 MHz elliptical niobium cavity, which is part of an ongoing study to assess the role of thermo-electric currents in flux trapping at the super conducting transition [1].

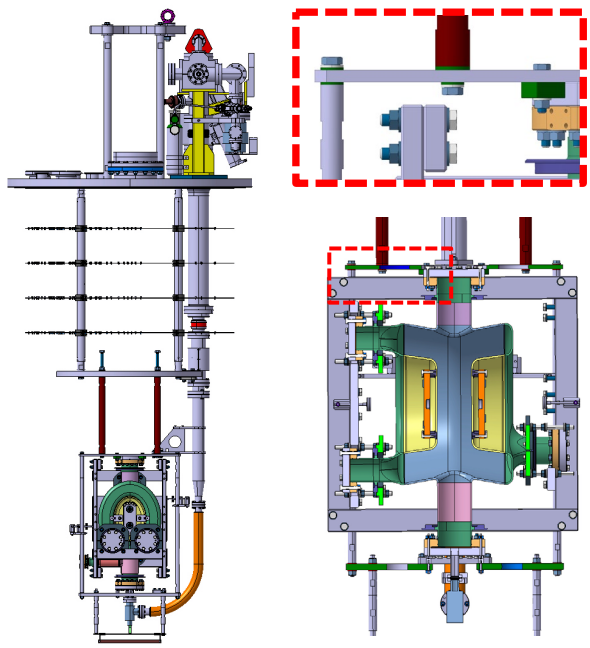

Figure 1: Cryostat insert with HL-LHC Crab cavity mounted. The cavity is electrically isolated from the insert by insulation washers (see zoom in), and is free standing with only a fixed point at the pumping line connection.

* niall.stapley@cern.ch

ISBN: 978-3-95450-211-0 doi:10.18429/JACoW-SRF2019-THP078

Traditionally cavity testing has been done with fixed input and pick-up antenna, with antenna length and design simulated prior to testing. While this was the simplest approach, a mobile coupler capable of operating at 2 K has now been designed and tested. With a stroke range of 50 mm, it allows for asserting critical coupling for the input antenna along the entire temperature range from 1.8 K-300 K. This offers improved multi-pacting conditioning over a larger temperature range, and also provides the possibility of improved monitoring of the cavity frequency during cool down.

The input antenna is also fitted with a DC bias system that permits the suppression/enhancement of multi-pacting in the input antenna vicinity. By monitoring the DC dark current from the antenna, both coupler and cavity conditioning can be clearly observed and addressed by application of a DC bias (up to 500 V).

For the RF input line, transient phase change of the reflected signal is used to monitor the VSWR ratio at the cryostat insert, in order to identify onset of feed through burnout. Recent experience has shown that with an input line of 7/8" coax, and a typical cryostat helium pressure of ~31 mBar, Paschen-induced breakdown at the warm feed through on the cryostat top-plate can be expected for RF input power in excess of 220 W. To reduce risk of feed through burnout, the RF line length inside the cryostat is set on a cavity-by-cavity basis so to minimise the VSWR for an off-resonance cavity.

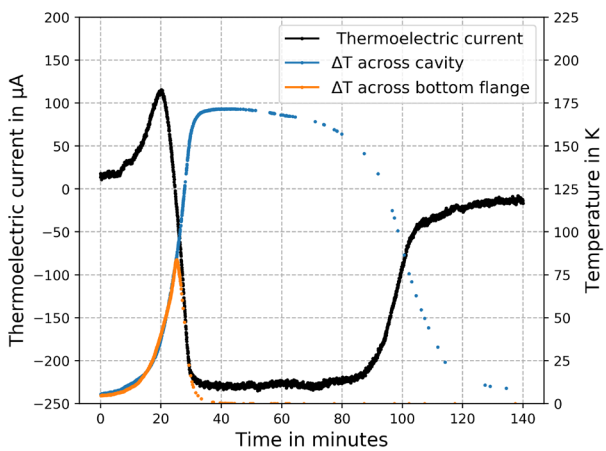

Figure 2: Measurement of thermal electric current flowing in the cavity/insert structure during cavity cool down.

LLRF SYSTEM

For RF measurements, the LLRF system is based on a modified digital LLRF module used for CERN's LHC, HIE-ISOLDE and LINAC4 installations [2] and offers both self-excited loop (SEL) and generator driven (GD) modes of operation. The system relies on user defined operating and sampling frequencies, and so has the capability of covering operating frequencies ranging from 100 MHz to 1.5 GHz.

Typically, the SEL mode is used for cavity validation conditioning when there is no precise target constraint on the cavity fundamental frequency. For test scenarios such as tuner validation and beam operation sequence testing, where precise control of the resonance frequency is required, the LLRF system is switched to GD mode and is operated in a way that mimics foreseen accelerator operations.

Being a fully digital system, the LLRF comes with observation memory for analog to-digital converters (ADCs) recording forward, reflected and transmitted power, which permits analysis of both transient and steady state cavity behavior in both pulse mode and continuous wave powering. The memory operates as a triggered ring buffer with space for 2^{20} 14-bit integer values on each of the measurement channels, and outputs magnitude and phase or I/Q of the digitized voltage signals. Further, a user defined decimation is implemented such that the full range of the memory buffer can span time windows from 0.5 to ~60 seconds.

For critically coupled SRF cavities with filling times of order 0.3-1.0 seconds, the system is typically operated in pulse mode with a pulse repetition frequency of 0.2 Hz. At this repetition rate the full data buffers for forward, reflected and transmitted can be read and processed, with the processing time only constrained by the buffer depth and the backplane transfer speed of the VME architecture used.

For each pulse, the measurement data are processed and recorded, and the quality factor Q_0 and cavity gradient E_{acc} evaluated. As an example, Fig. 3 shows a typical powering pulse and associated measurement points. Here it is noted that a pre-pulse is used in order for the SEL to lock on to the cavity resonance at low input power, immediately prior to the high-power pulse. This pre-pulse is particularly useful for cavities that expect large Lorentz force detuning, as it ensures that the SEL is then locked on resonance.

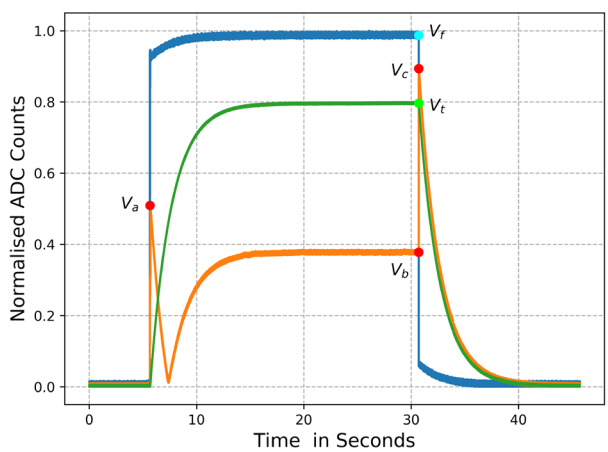

Figure 3: Digitised pulse measurement of a Niobium 5-cell 704 MHz cavity; pulses displayed are in terms of re-scaled ADC counts and are not representative of the real voltage levels. Traces show the forward (blue), reflected (orange) and transmitted (green) voltage signals coming from the cavity, and measurement points used for standard pulse analysis are marked with dots.

ISBN: 978-3-95450-211-0 doi:10.18429/JACoW-SRF2019-THP078

As can be seen from Fig. 3, the digitised pulse mode measurements are "text book" in form, and from the reflected pulse it is easily verified that the phase is well adjusted (i.e. for this over-coupled cavity, the reflected power drops to zero after pulse on). Indeed, for scanning the cavity across a range of powers, an initial pulse is used to validate the phase setting prior to the issuing of measurement pulses.

The digitisation in Fig. 3 represents the voltage signal as measured and each signal has noise from the cavity system as well as digitisation noise. For steady state signals, errors are reduced due to averaging over short segments of the high granularity buffer and suppression of least significant bit noise from the digitisation. For transient behaviour such as the value of the reflected power at pulse on/pulse off, linear regression fitting of the signal with is applied. Typical measurement errors are mainly from digitisation with noise levels of 10 counts on a full dynamic range of 20000 counts.

For each pulse, key measurement points (V_a, V_b, V_c, V_f, V_t) are taken and converted to relative power strengths (P_a, P_b, P_c, P_f, P_t). Calibrated cable-attenuated-corrected power signals ($P_F = c_f.P_f$, $P_R = c_r.P_r$ and $P_T = c_t.P_t$) are easily obtained when necessary, after determination of the appropriate cable attenuation on the signal path, but where possible RF measurement quantities are determined from the relative power signals, in order to minimise systematic error contributions.

MEASUREMENTS AND RESULTS

With the majority of measurements done in pulse mode, measurement procedures are defined in terms of modular tasks assembled into sequences. These sequences are assembled via a standard scripting interface to provide automated measurement procedures. Examples of modular tasks include the issuing and measurement of a pulse, optimisation of the SEL phase, and processing of measurement buffers. Standard Q_0 vs E_{acc} scans are then defined simply as a pulse sequence at varying pulse power levels, with SEL phase optimisation at each power step.

The advantage of this modular task approach combined with a high-level scripting framework is that the user can easily put together and test sequences and semi-intelligent algorithms catering to the adaptive tasks such as cavity conditioning and multi-pacting processing.

For RF performance measurements of a cavity, the test stand is first calibrated by measuring the exponential decay of the power signal from the cavity pickup, and the quality factors of the input and pickup antenna, Q_e, Q_t, are determined. Using the digitisation of the pulses as shown in Fig.3, identified measurement points are evaluated, which permits the calculation of the input and pickup couplings β_e and β_t and then Q_e, Q_t via the standard expressions [3].

$$\beta_e = \frac{P_c}{P_a(1-\epsilon)-P_b} \quad \text{where} \quad \epsilon = |P_T/P_F|$$

$$\beta_t = \beta_e \, \epsilon \frac{P_a}{P_c}$$

$$Q_e = \frac{1+\beta_e+\beta_t}{\beta_e}\,\omega\tau \quad \text{and} \quad Q_t = \frac{1+\beta_e+\beta_t}{\beta_t}\,\omega\tau$$

For fixed antennas, Q_e and Q_t, are physical constants and define the configuration of the test setup.

Pulse scans at increasing power can then be performed, and the Q_0, cavity stored energy U, and accelerating gradient E_{acc} determined following:

$$U = k\,P_T \quad \text{where} \quad k = Q_t/\omega$$

$$E_{acc} = \sqrt{U/\kappa}$$

with $\omega = 2\pi f$ and κ is the conversion factor obtained from electromagnetic simulations.

For Q_0, each digitized pulse can be fitted to determine the time constant of the power decay of the individual pulse, and then Q_0 is extracted.

$$Q_0 = \frac{1}{\frac{1}{\omega\tau_i} - \frac{1}{Q_e} - \frac{1}{Q_t}}$$

Alternatively, Q_0 can be evaluated from

$$Q_0 = \frac{\omega U}{P_0}$$

Here P_0 is the power absorbed by the cavity, and can be determined by

$$P_0 = \frac{P_a - P_b}{P_a} P_F - P_T \quad \text{or} \quad P_0 = P_F - P_R - P_T$$

For precision scans the approach of individual fitting of the time constant of the power decay is preferred, while for statistics, evaluation of Q_0 from U can be done using a reduced set of 5 measurement points (P_f, P_t, P_a,P_b,P_c). This data-reduction step retains sufficient accuracy and permits pulse-by-pulse processing and storage. Unreduced single pulse data buffers are ~100MB per pulse, making extended storage of raw pulse-by-pulse data unrealistic. As such, real-time pulse processing and reduction of pulse-by-pulse data are implemented by default.

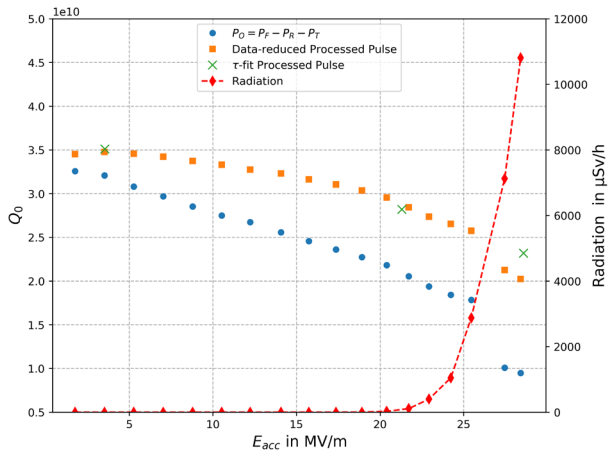

Figure 4: Comparison of pulse processing techniques used to assess RF performance. Data shown is for a 704 MHz 5-cell elliptical cavity measured at 2.0 K.

Figure 4 shows the comparison of the three pulse-processing methods, and shows that the evaluation of P_0 by

ISBN: 978-3-95450-211-0 doi:10.18429/JACoW-SRF2019-THP078

$P_0 = P_F - P_R - P_T$ is considered more susceptible to system and calibration error contributions from the measurement of the three absolute power values.

As the LLRF system buffer contains amplitude and phase information for forward, reflected and transmitted power, phase monitoring of relative phase change can be used to assess transient behaviour on the cavity. For example, cavity quench measurements on HL-LHC crab cavities have been analysed via observed phase shifts on the cavity pickup to give not only the Lorentz force detuning, but also the expected beam sensitivity to cavity quenches [4]. As part of this work Fig. 5 shows the pressure detuning associated with a cavity quench of an HL-LHC crab cavity prototype.

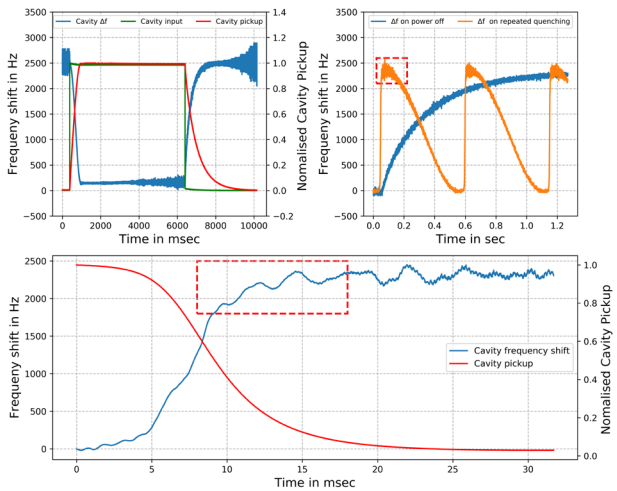

Figure 5: Frequency shifts as extracted from the derivative of the phase signal coming from the pickup antenna of an HL-LHC Crab cavity prototype measured at 1.8 K. Top left show the Lorentz Force detuning on application of a 6 second pulse. The cavity does not quench but is clearly showing stability issues in the latter part of the pulse. Top right compares the frequency response of a normal pulse off (blue) to repeated quench and recovery of the cavity (orange). The bottom plot is a zoom in of the frequency response of the quench where we see frequency oscillations due to pressure detuning [4].

TEST STAND BENEFITS

The choice of framework implementation has been such that the test stand mirrors CERN-standard accelerator controls system [5]. This choice is based on hardware/firmware separated from the user interface by a controls middle layer (see Fig. 6) and uses a standard device/property model. Such a structure permits the full integration of a configuration database, seamless integration of real-time control and measurement data across a variety of hardware types, as well as standardized logging of control operations, interlocks and measurement data. Being based on CERN accelerator controls standards, the controls framework streamlines the introduction of new sensors and devices, and with support from in-house operations teams, development costs are kept to a minimum. Coupled with standard utilities for debugging and development, along with RF specific libraries and analysis packages integrated into this middleware, this allows the RF tester to maintain full flexibility to work either in a production-level testing or a rapid development environment. To facilitate understandable development all user defined routines and sequences are written as Python methods.

This data acquisition architecture enables the acquisition of RF measurement data based on processed data-reduced LLRF buffer, but with synchronized snapshots of environmental data attached, which has proved invaluable for transient phenomena studies. Due to the interlaced nature of the RF data and the environmental snapshots, the HFDF5 [6] hierarchical data format to permit user readability of the pulse-by-pulse measurements under varying conditions is used for permanent storage. In parallel, full environmental data is logged to a central database at 1Hz, and is used as a reference for interfacing services and providers external to the RF cavity testing team.

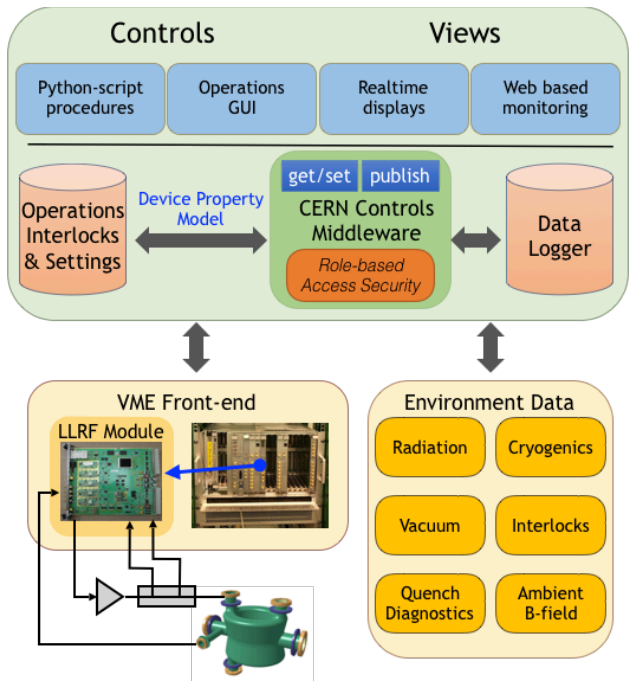

Figure 6: Architectural layout of the test stand, based on standard CERN accelerator infrastructure and a device property middleware layer.

With this software architecture and the use of standard accelerator tool sets, the test stand ensures full production-level deployment with full version control, while still retaining development flexibility by means of the python interpreter embedded in the middleware. This coupled with INSPECTOR, an in-house graphical user interface [7], permits rapid and consistent deployment of measurement sequences, operator consoles (Fig. 7), and web-based monitoring channels.

Finally, it is noted that the costs for such a system are kept low, as it is based on CERN-standard and supported

ISBN: 978-3-95450-211-0 doi:10.18429/JACoW-SRF2019-THP078

accelerator RF hardware modules and infrastructure, combined with open source software that permits transparent development without hidden proprietorial costs.

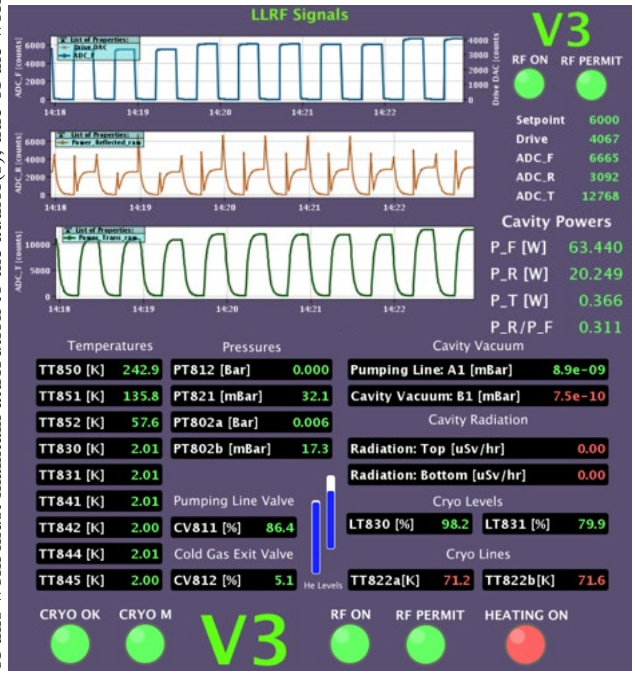

Figure 7: Example of a standard user interface for both RF measurements and cold test environmental data. These interfaces have been developed using the CERN-developed open source INSPECTOR application [7].

OUTLOOK

The test stand framework is now deployed and fully operational on two large volume cryostats in CERN's SRF test facility, and is to be used for production testing of crab cavities for the HL-LHC program [8], starting in mid-2019.

With the hardware and software infrastructure now implemented, focus is shifting to development of algorithms and test sequences specific to cavity RF performance, conditioning and validation. As part of this, the integrity of the test stand is now forefront when introducing changes, with both individual and full end-to-end testing required. For end-to-end testing the requirement of validating with a cold cavity has been a limiting factor, and to avoid this constraint, a generic cavity simulator is being integrated into the test stand framework. This simulator uses a simple cavity model [9] downloaded into an off the-shelf, low-cost, open-source compatible FPGA development board [10].

In addition, for studying fast transient phase changes coupled with longer-term cavity response an "Obs-box" [11] is being integrated. This is a CERN-developed diagnostic system to overcome the limitations of the VME bus transfer-time, that delivers unfiltered and undecimated data buffers with millisecond level streaming, and will permit full high-resolution studies of cavity behavior in both quasi-steady state and transient modes.

ACKNOWLEDGEMENTS

The authors would like to thank Daniel Valuch and Michael Elias for both providing and helping adapt their LLRF design to our use case.

We would also like to thank Rob Apsimon (Lancaster University) for ongoing help and support with the cavity simulator software model.

REFERENCES

[1] A. Ivanov, A. Macpherson, and F, Gerigk, "Direct measurement of Thermoelectric currents during cooldown", presented at the SRF2019 Dresden, Germany, July 2019, paper THP094, this conference.

[2] D. Valuch and M.Elias, "RF system for the HIE-ISOLDE", HIE-ISOLDE Workshop: The Technical Aspects, November 2103 CERN, https://indico.cern.ch/event/255042/

[3] I. Ben-Zvi, "SRF Cavity Testing with a Self-Excited Loop", May 2018, CERN-ACC-Note-20180039.

[4] R. Apsimon, G. Burt, A. Dexter, N. Shipman, A. Castilla, A. Macpherson, K. Ness Sjobak, A. Santamaria Garcia, N. Stapley, A. Alekou, and R. B. Appleby, "Prediction of beam losses during crab cavity quenches at the high luminosity LHC", Phys. Rev. Accel. Beams **22**, 061001, June 2019.

[5] R. Gorbonosov, "The Control Systems of the Large Hadron Collider", Academic Training Lecture Regular Programme, Oct. 2013, https://indico.cern.ch/event/273998/

[6] HDF5, https://portal.hdfgroup.org/display/support

[7] V. Costa and B. Lefort, "Inspector, a Zero Code IDE for Control Systems User Interface Development", in *Proc. 16th Int. Conf. on Accelerator and Large Experimental Control Systems (ICALEPCS'17)*, Barcelona, Spain, Oct. 2017, pp. 861-865. doi:10.18429/JACoW-ICALEPCS2017-TUPHA184

[8] G. Apollinari, I. Béjar Alonso, O. Brüning, P. Fessia, M. Lamont, L. Rossi, L. Tavian, "High-Luminosity Large Hadron Collider (HL-LHC) Technical Design Report V0.1", April 2017, CERN-2017-007-M (CERN Yellow Reports: Monographs, 4/2017.

[9] R. Apsimon (Lancaster University), "Cavity Simulator models", private communication.

[10] Red Pitaya, https://www.redpitaya.com

[11] M. Ojeda Sandonís *et al.*, "Processing High-Bandwidth Bunch-by-Bunch Observation Data from the RF and Transverse Damper Systems of the LHC", in *Proc. 15th Int. Conf. on Accelerator and Large Experimental Control Systems (ICALEPCS'15)*, Melbourne, Australia, Oct. 2015, pp. 841-844. doi:10.18429/JACoW-ICALEPCS2015-WEPGF062